Available online at www.sciencedirect.com
SCIENCE DIRECT
Polymer 46 (2005) 4714–4721
polymer
www.elsevier.com/locate/polymer

Self-assembly of C_{60} containing poly(methyl methacrylate) in ethyl acetate/decalin mixtures solvent

Palaniswamy Ravi[a], Sheng Dai[a], Khan Meng Hong[a], Kam Chiu Tam[a,b,*], Leong Huat Gan[c]

[a]*Singapore-MIT Alliance, 50 Nanyang Avenue, 639798 Singapore, Singapore*
[b]*School of Mechanical and Aerospace Engineering, Nanyang Technological University, 50 Nanyang Avenue, 639798 Singapore, Singapore*
[c]*Natural Sciences, National Institute of Technology, Nanyang Technological University, 50 Nanyang Avenue, Singapore 637616, Singapore*

Received 13 January 2005; received in revised form 8 March 2005; accepted 23 March 2005
Available online 19 April 2005

Abstract

[60]Fullerene (C_{60}) was mono-substituted with well-defined poly(methyl methacrylate) (PMMA-*b*-C_{60}) using the atom transfer radical polymerization (ATRP) technique. The self-assembly behaviors of PMMA-*b*-C_{60} in ethyl acetate (EA) and decalin mixtures were studied using laser light scattering (LLS) and transmission electron microscopy (TEM). Homogeneous solutions of PMMA-*b*-C_{60} can be obtained in the solvent mixtures containing more than 40 wt% EA, where the molar ratio of decalin to EA is close to 1. For each solvent mixture, unimers coexist with micelles and large aggregates. The sizes of PMMA-*b*-C_{60} micelles and aggregates are independent of polymer concentration, confirming that they are produced via the closed association mechanism. For the various solvent mixtures, the weight-averaged molecular weights, M_w of the PMMA-*b*-C_{60} aggregates range from 4.1×10^7 to 12.5×10^7 g/mol. The hydrodynamic radii of the large aggregate, R_h, vary from 90 to 136 nm, while the *z*-averaged radii of gyration, R_g, range from 210 to 311 nm. The R_g/R_h value for each solvent mixture is ~2.3, which is independent of decalin contents in the mixed solvents. The morphological study using the transmission electron microscope suggests that the large aggregates are composed of porous large compound micelles (LCM) in solution.

Keywords: [60]Fullerene (C_{60}); Large compound micelle; ATRP

1. Introduction

Since the discovery of [60]fullerene (C_{60}), much research work has been devoted to C_{60} due to its unusual symmetry and variety of interesting properties [1–3]. However, many of its potential applications have been seriously hampered by its poor solubility and processability [4]. One way to overcome this problem is to synthesize fullerene derivatives by introducing surfactants or long chain polymers [5–7]. Another way of increasing the solubility of fullerene is to form charge transfer complexes using electron donor–acceptor interactions [8–10]. In recent years, researches on the C_{60} containing polymers have intensified since these polymers are soluble in common organic solvents. Polymers that are covalently bound to the fullerene are potentially useful for many different applications [11,12]. Some progress has been made on the synthesis of well-defined C_{60} end-capped polymers [13,14]. These types of fullerene conjugated with well-defined polymers could form nano-scale aggregates in organic solvents or in aqueous solutions [15]. Developments of different morphology in the aggregates and its aggregation mechanism in solution using well-defined polymeric system are of potential interest to the research community. For C_{60} containing polymer, the chemical structure, the molecular weight and the concentration of polymer together with the solvent quality play important roles in controlling the morphology of the aggregates [16]. Until recently, there are only a few papers describing the aggregation behavior of fullerene containing polymers in solution. Lately, C_{60} end-capped poly(ethylene oxide)s were synthesized and large spherical-like compound aggregates were observed in polar solvents [17]. The bola-amphiphilic C_{60} containing two ammonium head groups was synthesized and the aggregation behavior in aqueous solution confirmed the

* Corresponding author. Address: School of Mechanical and Aerospace Engineering, Nanyang Technological University, 50 Nanyang Avenue, 639798 Singapore, Singapore. Fax: +65 6791 1859.
E-mail address: mkctam@ntu.edu.sg (K.C. Tam).

0032-3861/$ - see front matter © 2005 Elsevier Ltd. All rights reserved.
doi:10.1016/j.polymer.2005.03.061

formation of vesicle-like structure [18]. C_{60} grafted with two well-defined polystyrene or poly(*p*-vinylphenol) arms were synthesized and the micellization behavior in THF was examined [19]. Stable micelles with aggregation number ranging from 6 to 20 were obtained by varying the amounts of –OH substitution. Wang et al. studied the micellization behavior of fullerene containing poly(alkyl methacrylate)s in THF and reported the existence of individual polymer chains with core-shell aggregates [20]. Yang and co-workers just reported the aggregation behavior of poly-(acrylic acid)-*b*-C_{60} in aqueous solution with core-shell like structure and the microstructure dominates the photo-conductive properties [21].

Only few studies have focused on the solution properties of this unique class of C_{60} containing polymers, and fundamental understanding of the micellization behavior is still not very clear. New types of morphological aggregates could be produced using the solvent-induced micellization technique. From literature, there is a scarcity of report on the solvent induced aggregation behavior of well-defined fullerene containing polymers. In this study, a well-defined mono-substituted [60]fullerene containing poly(methyl methacrylate) was synthesized by atom transfer radical polymerization technique (ATRP). The aggregation behaviors of PMMA-*b*-C_{60} in the selective solvent mixture were studied using different techniques. Since ethyl acetate and decalin are selective solvents for PMMA and C_{60} respectively, PMMA-*b*-C_{60} in EA/decalin solvent mixture will self-assemble to produce interesting morphologies. The resulting aggregates were examined by laser light scattering (LLS) and transmission electron microscopy (TEM) techniques. Direct morphological investigation determined by TEM provides images of the aggregates could be used to validate the microstructure determined from LLS studies.

2. Experimental section

2.1. Materials

Methyl methacrylate monomer (MMA, Aldrich) was dried over CaH_2 and distilled under reduced pressure. [60]Fullerene (C_{60}, >99.5%, Materials Technologies Research Ltd) was used without further purification. CuCl and 1,1,4,7,10,10-hexamethyltriethylenetetramine (HMTETA) was purchased from Aldrich and used as received. Ethyl acetate (EA) and decalin were purchased from Merck and distilled prior to use.

2.2. Synthesis of PMMA–Cl macroinitiator

PMMA-*b*-C_{60} was synthesized using atom transfer radical polymerization (ATRP) technique according to the published report [22]. First, PMMA–Cl macroinitiator was synthesized using *p*-toluene sulfonyl chloride as an initiator and CuCl/HMTETA as a catalyst system (1:1:1 initiator:CuCl:HMTETA) in anisole at 90 °C. In a typical experiment, initiator (0.081 g, 4.25×10^{-4} mol), CuCl (molar equivalent to initiator), and magnetic bar were introduced into a pre-dried Schlenk flask and tightly sealed with rubber septum. Deoxygenated anisole (50 vol% with respect to monomer), followed by the monomer (5 ml, 0.0467 mol) were introduced into the flask via an Ar-washed syringe and stirred until the system became homogeneous. Three 'free-pump-thaw' cycles were performed to remove any oxygen from the polymerization solution. Finally, the degassed ligand (HMTETA, molar equivalent to initiator) was introduced using Ar purged syringe and placed in a thermostated oil bath at 60 °C. After 90% conversion (90 min) was attained, the reaction was stopped by diluting with THF. The catalyst was removed by passing through the alumina column and the polymer solution was concentrated and precipitated in large excess of methanol. The re-precipitation procedure was repeated three times using THF/methanol system and the polymer was dried under vacuum at room temperature. The number-averaged molecular weight of the well-defined PMMA–Cl macroinitiator determined from gel permeation chromatography (GPC) was 14,000 g/mol with M_w/M_n of $\sim$1.18.

2.3. Synthesis of PMMA-b-C_{60}

PMMA–Cl macroinitiator was used for the synthesis of mono-substituted PMMA with C_{60} (PMMA-*b*-C_{60}). The reaction was carried out in 20 ml of 1,2-dichlorobenzene using the same catalyst system (1:1:1, PMMA–Cl (2 g):CuCl:HMTETA) at 90 °C for 24 h. To avoid multiple grafting of the polymer on C_{60}, excess amount of C_{60} (0.308 g, molar ratio 3:1 C_{60}:macroinitiator) was used. After the reaction was completed, the solution was diluted with large amounts of THF (to remove unreacted C_{60}) and passed through the alumina column. The polymer solution was concentrated and precipitated into large excess of methanol. The polymer was re-precipitated by dissolving in THF, filtered and added drop-wise into large excess of methanol. This re-precipitation procedure was repeated three times in order to completely remove unreacted C_{60}. Finally, the polymer was dried under vacuum at room temperature. The molecular weight M_n of the PMMA-*b*-C_{60} is $\sim$14200 g/mol with $M_w/M_n\sim1.22$ as determined from GPC traces.

2.4. Gel permeation chromatography (GPC)

Agilent 1100 series GPC system equipped with a LC pump, PLgel 5 μm MIXED-C column, RI and UV dual detectors was used to determine polymer molecular weights and the molecular weight distributions. The column was calibrated with narrow molecular weight polystyrene standards. HPLC grade THF stabilized with BHT was used as a mobile phase. The flow rate was maintained at 1.0 ml/min. The absorption wavelength for the UV detector was set at 330 nm.

2.5. Thermogravimetric analysis (TGA)

Perkin–Elmer TGA7 thermogravimetric analyzer was used to carry out TGA measurements. Temperature was scanned from 25 to 800 °C with a scan rate of 10 °C/min under N_2 flow.

2.6. Laser light scattering

Brookhaven BI-200SM goniometer system equipped with a 522 channel BI9000AT digital multiple τ correlator was used to perform static and dynamic light scattering experiments. A 0.45 μm PTFE filter was used to remove dust prior to the light scattering measurements. For static light scattering (SLS), Berry plot was used to analyze the experimental data, and the refractive index increments, d*n*/d*C*, were measured using a BI-DNDC differential refractometer. For dynamic light scattering (DLS), the inverse Laplace transform of REPES in the Gendist software package was used to analyze the time correlation functions with probability of reject setting at 0.5. The refractive index and viscosity of the mixed solvents were measured using Atago 3T Abbe refractometer and LS40 control rate rheometer respectively.

2.7. Transmission electron microscopy

A JEOL JEM-2010 TEM was used to obtain the micrographs, which operates at an accelerating voltage of 200 kV. A drop of solution was placed onto a 200 mesh copper grid pre-coated with Formvar and carbon. The samples were dried under vacuum before measurements.

3. Results and discussion

3.1. Polymer characterization

The detailed synthesis procedure for PMMA-*b*-C_{60} is shown in Scheme 1. PMMA-*b*-C_{60} was synthesized using ATRP technique as described previously [22]. However, different initiator and catalyst systems were used to obtain stable active end-groups of the PMMA macroinitiator. From our previous experience, the use of bromine based initiator (ethyl 2-bromoisobutyrate) and CuBr catalyst for the methacrylate systems resulted in the loss of active end-groups [23]. In this study, we used *p*-TsCl initiator in the presence of CuCl/HMTETA catalyst system in anisole to produce PMMA with stable active –Cl end-groups. For mono-substituted C_{60} conjugated PMMA, similar ATRP condition was used. The polymerization was carried out in 1,2-dichlorobenzene with molar ratio of C_{60}:PMMA ~3:1 to avoid the multiple substituted products. GPC traces of the synthesized PMMA–Cl and PMMA-*b*-C_{60} using RI detector showed a mono-model distribution (Fig. 1) without significantly altering the molecular weight and polydispersity (1.18 for PMMA–Cl and 1.22 for PMMA-*b*-C_{60}). The comparison of the PMMA-*b*-C_{60} GPC traces using either UV or RI detector shows similar elution time, which confirms that C_{60} has been conjugated to PMMA chains. GPC traces using RI and UV detectors as shown in Fig. 1 confirmed the formation of mono-substituted product since the UV detector only responds to the C_{60} moiety in the fullerene containing polymer (PMMA-*b*-C_{60}) [24]. However, a slight shoulder peak was observed from the UV detector, which is possibly related to the absorption phenomena rather than size exclusion due to the fact that the UV absorption is sensitive to the concentration of absorbent. Also, there may be trace amounts of un-reacted PMMA homopolymer, which is not possible to remove, but we believe the self-assembly property of the PMMA-*b*-C_{60} polymer will not be significantly altered.

To further verify the conjugation of C_{60} to the PMMA chains, UV–vis spectroscopy of the PMMA-*b*-C_{60} in ethyl acetate was studied and shown in Fig. 2. We observed clear evidence of C_{60} absorption peak at 335 nm, which confirmed that C_{60} was covalently attached to PMMA. The insert shows some difference in absorption spectra in the visible wavelength region. The spectra is less structured and no pronounced maxima were observed, which strongly supports the successful conjugation of PMMA chains onto C_{60}, which perturbs the conjugated structure and the electronic properties of C_{60} molecules. This is also reinforced by the change in the color of the solution from purple (C_{60}) to yellow (PMMA-*b*-C_{60}). In addition, no obvious absorption at 514 nm was observed, which indicates that the grafting of PMMA to C_{60} is a 1,2-addition, and not a 1,4-addition.

Themogravimetric analysis (TGA) was further used to evaluate the grafting ratio of C_{60} onto PMMA chain since all PMMA decomposed before 550 °C and C_{60} is still stable until 600 °C [22]. The calculated amount of C_{60} is ~5 wt%, which agrees with the theoretical values. The TGA result further confirmed the formation of mono-substituted product.

3.2. Laser light scattering

Dynamic light scattering (DLS) was used to study the aggregation behavior of PMMA-*b*-C_{60} in ethyl acetate (EA)/decalin mixed solvents at various concentrations. Since the solvent selective properties of the PMMA-*b*-C_{60} polymer for ethyl acetate and decalin are different, aggregates or micelles are produced in EA/decalin mixed solvents. However, due to the long PMMA chains compared to C_{60} molecules, the polymer is insoluble in the solvent mixture when the decalin content is greater than 60 wt%. The critical micellization concentration (CMC) of PMMA-*b*-C_{60} in the solvent mixture was detected by recording the polymer concentration dependence of the scattered light intensity of polymer in different solvent mixtures. Although scattering light intensity decreases with decreasing polymer

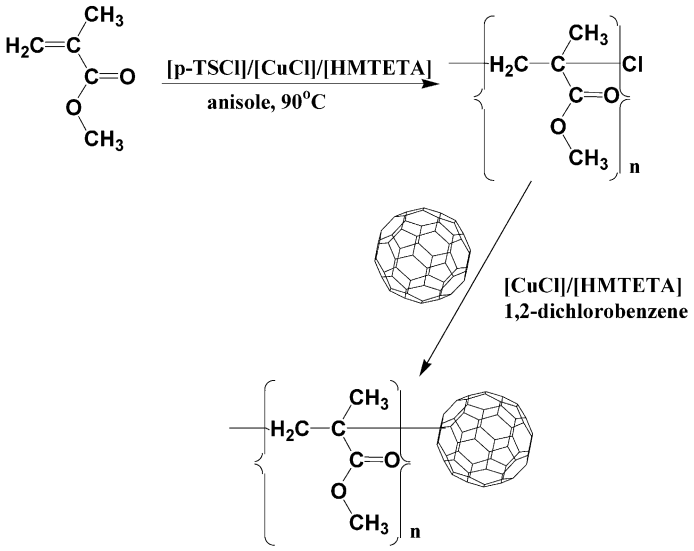

Scheme 1. Synthesis scheme of PMMA-*b*-C_{60} using ATRP.

concentration, an abrupt transition cannot be detected even at a PMMA-*b*-C_{60} concentration of 0.008 wt%. After analyzing the time correlation function (TCF), small amount of aggregates were still detectable. It can be concluded that CMC was extremely small for the present system.

One decay mode is evident in the decay time distribution function of 1 wt% PMMA-*b*-C_{60} in 100 wt% EA measured at 25 °C. However, for the polymer in the solvent mixtures, the slow decay mode co-exist with two small fast decay modes in the decay time distributions and they shift to lower decay times with increasing scattering angles. All decay rates Γ exhibit good linear relationship with q^2, suggesting that these decay modes are caused by the translational diffusion of three different types of particles in solution. Under this condition, the decay time is proportional to the apparent hydrodynamic radius R_h of the particle in dilute solution. In order to understand the true R_h values of these three components and the association mechanism, DLS was carried out on different concentrations of PMMA-C_{60} system (0.1, 0.2, 0.3, 0.4 and 0.5 wt%) to determine the concentration dependence of the translational diffusion coefficients. Fig. 3 shows a typical decay time distribution obtained for different polymer concentrations in the solvent mixture containing 70 wt% EA, where the decay times or translational diffusion coefficients are independent of polymer concentration, which indicates the closed association model and the apparent R_h is independent of polymer concentration. Based on Stokes–Einstein expression, the hydrodynamic radius R_h could be determined from,

$$R_h = \frac{kT}{6\pi\eta_0 D_0} \tag{1}$$

where k isthe Boltzmann constant, η_0 the viscosity of the solvent, and T the absolute temperature. D_0 is the diffusion coefficient at infinite dilute solution. The R_h values determined from the Stokes–Einstein equation for the fastest mode were between 1 and 3 nm for various polymer concentrations, which should correspond to PMMA-*b*-C_{60} unimers. Similarly, the R_h values determined for the intermediate mode are in the range between 10 and 20 nm, which corresponds to core-shell micelles. The R_h value determined for the dominant slow mode is ~106 nm for the solvent mixture containing 70 wt% EA and the sizes of the aggregates are independent of polymer concentrations. The values of R_h for the various solvent mixtures are summarized in Table 1.

Since scattered light is more sensitive to large particle in solution, the large aggregates dominate the decay time distribution function. Due to the fact that the decay time distribution is the intensity-averaged distribution, the amount of the aggregates is lower than that of unimers and micelles.

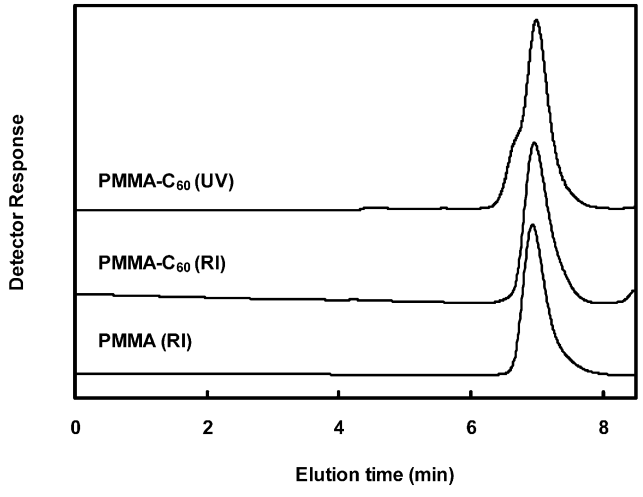

Fig. 1. GPC traces of (a) PMMA macroinitiator (RI), (b) PMMA-*b*-C_{60} (RI), and (c) PMMA-*b*-C_{60} (UV).

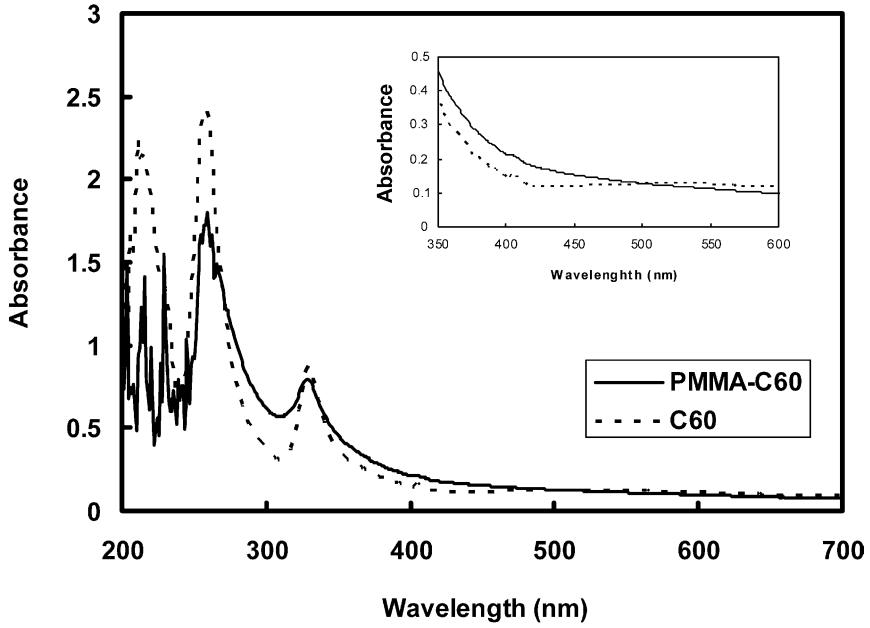

Fig. 2. UV–vis spectroscopy of C_{60} in cyclohexane, and PMMA-*b*-C_{60} in ethyl acetate.

Static light scattering (SLS) was also used to study the aggregation behavior of PMMA-*b*-C_{60} in different ethyl acetate/decalin mixtures. Using the SLS, one can determine the *z*-averaged radius of gyration (R_g) and weight averaged molecular weight of the particles in solution. Due to the strong intermolecular interaction for the current system, Berry-plot was more suitable to determine the weight-averaged molecular weight M_w and R_g instead of the widely used Zimm-plot

$$\left(\frac{KC}{R_\theta}\right)^{0.5} = \left(\frac{1}{M_w}\right)^{0.5}\left(1+\frac{1}{6}q^2R_g^2\right)(1+A_2M_wC) \qquad (2)$$

where $K\,(=4\pi^2n^2(\mathrm{d}n/\mathrm{d}C)^2/N_A\lambda^4)$ is an optical constant with N_A, n, and λ being the Avogadro's number, the solvent refractive index, and the wavelength of the light in vacuum, respectively. dn/dC is the refractive index increment of the polymer solutions obtained from the differential refractometer, C is the polymer concentration, R_θ is the excess Rayleigh ratio, M_w is the weight-averaged molar mass, and R_g is root-mean square *z*-averaged radius of gyration. A_2 is the second viral coefficient, and q is the scattering wave vector $(=4\pi n\sin(\theta/2)/\lambda)$, θ is the scattering angle. The values of the refractive index increment dn/dC of PMMA-*b*-C_{60} in different solvent mixtures determined from BI-DNDC differential refractometer are summarized in Table 1.

Fig. 4 shows the typical Berry-plot for PMMA-*b*-C_{60} in 65 wt% EA with polymer concentration ranging from 0.1 to 0.5 wt%. The weight-averaged molecular weight M_w was determined to be 4.08×10^7 g/mol. The averaged aggregation number could be determined by the quotient of the

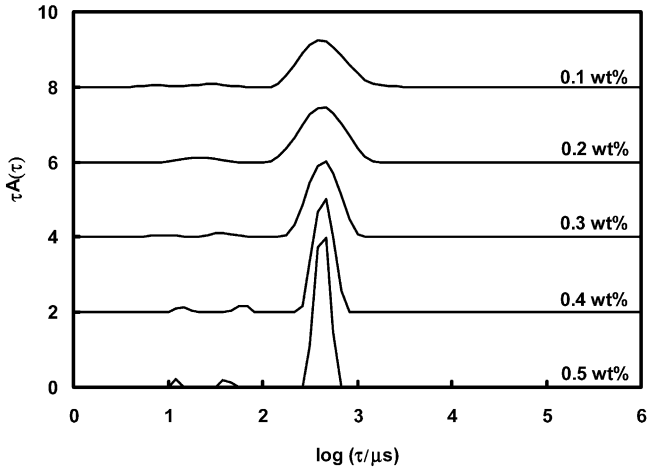

Fig. 3. The decay time distribution functions for different concentrations of PMMA-*b*-C_{60} in 70 wt% EA solvent mixture measured at 25 °C.

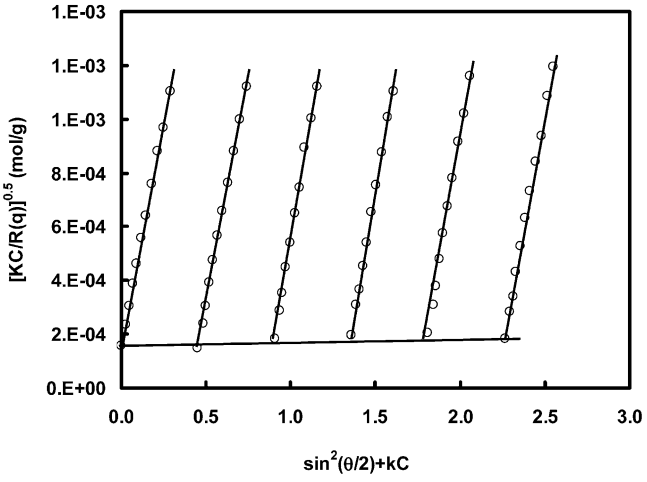

Fig. 4. Berry plot of PMMA-*b*-C_{60} in 65 wt% EA solvent mixture with polymer concentration ranging from 0.1 to 0.5 wt%.

Table 1
Summary of laser light scattering data for PMMA-*b*-C_{60} in EA–decalin mixed solvents at 25 °C

EA content (wt%)	Viscosity (10^{-4} Pa s)	Refractive index	d*n*/d*C*	Fraction[a] (%)	R_h[b] (nm)	R_g (nm)	R_g/R_h[b]	M_w (10^7 g/mol)
65	5.89	1.4070	0.0944	93.9	131	311	2.37	4.1
70	5.58	1.4008	0.0940	93.2	106	244	2.30	4.3
75	5.19	1.3954	0.0936	94.4	136	299	2.20	4.7
80	5.06	1.3916	0.0934	93.1	111	264	2.38	6.0
90	4.63	1.3810	0.0926	95.3	90	210	2.28	12.5
95	4.51	1.3764	0.0923	97.4	121	276	2.28	12.5
100	4.14	1.3712	0.0919	96.6	111	257	2.32	14.0

[a] Fraction of LCM.
[b] R_h obtained from the slowest mode in the decay time distributions, which corresponds to the R_h of LCM in solution.

aggregate M_w and the unimer M_w. Since there are three types of particles in solution, the calculated weight-averaged aggregation number is only an apparent value. It is found that the apparent aggregation number N_{agg} was about 2458. At the same time, the *z*-averaged radius of gyration (R_g) was found to be 311 nm. Since the R_h values of both unimers and micelles compared to that of aggregates from DLS studies, the main contribution to the *z*-averaged R_g is attributed to the aggregates. However, the coexistence of unimers and micelles leads to the increase in the polydispersity. Table 1 summarized the values of R_h of the slow mode, R_g, R_g/R_h and M_w obtained for PMMA-*b*-C_{60} for other solvent mixtures.

Fig. 5 shows the comparison of R_h, R_g and R_g/R_h for PMMA-*b*-C_{60} at various solvent mixtures at 25 °C. R_h and R_g values of the nano-particles vary within a narrow band, indicating that the dimensions of the particles remain unchanged within the experimental solvent mixture range. The combination of DLS and SLS, R_g/R_h can be used to examine the probable morphology of the aggregates. The calculated ratio of R_g/R_h for PMMA-*b*-C_{60} in 65 wt% EA was 2.37, which is independent of solvent ratios and remains within the range of 2.20–2.38. The higher R_g/R_h value indicates a dominant draining effect in the structure of the aggregates. In addition, the higher polydispersity also give rise to the increase in the R_g/R_h value. Based on the chemical structure, solvent selectivity and observed large particle size, we proposed that the aggregates are likely to be porous-like large compound micelles (LCM), comprising of many regular core-shell micelles. These LCMs are in dynamic equilibrium with the unimers and micelles. In addition, the LCM becomes more stable with increasing polymer concentration as evident from Fig. 3, where the modes of the LCM become narrower and more well-defined with increasing the polymer concentration. The polydispersity index (PDI) was computed for each polymer concentration based on the Cumulant analysis and plotted against the solvent composition, where the PDI decreases from 0.34 to 0.24 with increasing polymer concentration. With increasing polymer concentration, it is thermodynamically more favorable to produce large aggregate, which co-exist with unimers and micelles. Such trend correlates with the observation in Fig. 3 that the continuous decay time distribution were found to be substituted by the well-separated decay time distribution at high PMMA-*b*-C_{60} concentration. Similar trend was reported for a tri-block copolymer consisting of styrene and 5-(*N*,*N*-diethylamino)isoprene in 100% dioxane and also in 100% tetrahydrofuran system [25].

In addition, the weight-averaged molecular weights (M_w)

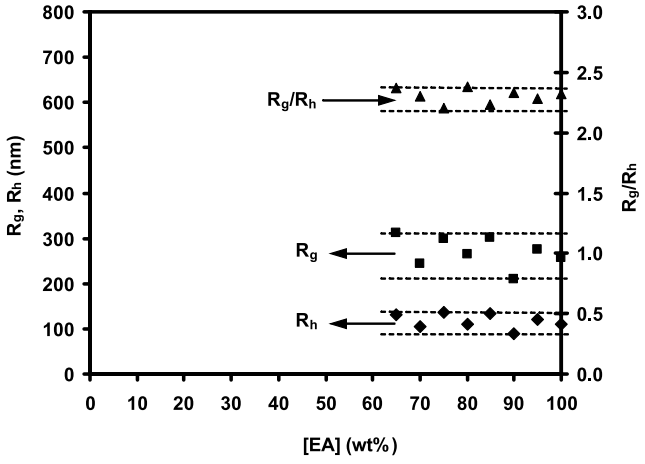

Fig. 5. Comparison of R_h, R_g and R_g/R_h for PMMA-*b*-C_{60} at various solvent mixtures measured at 25 °C.

of the LCM decrease with increasing the proportion of decalin in the solvent mixtures, without any observable increase in the particle size. This interesting behavior can be explained by the lyophobic and lyophilic character of C_{60} core in various solvent mixtures. In 100% EA, C_{60} forms compact micellar core due to the fact that C_{60} is lyophobic to EA, while the PMMA segments is lyophilic to EA which form the outer corona layer. When increasing the ratio of decalin/EA, some of the decalin molecules are solvated in the C_{60} core (being a good solvent for C_{60} and a poor solvent for PMMA), resulting in the swelling of the lypophilic C_{60} micellar core, which increases the overall size of individual micelle in the LCM. However, the size of the LCM does not change, which suggesting that fewer individual micelles are incorporated in the LCM as confirmed by the lower molecular weight of the LCM in 65 wt% EA. Fig. 6 gives a pictorial representation of the aggregation behavior of PMMA-*b*-C_{60} in different solvent mixtures.

When the proportion of decalin reaches a critical level where decalin molecules begin to displace the EA molecules solvated within the PMMA chains, the PMMA-*b*-C_{60} unimers become insoluble in the solvent mixture and precipitate out, which explained the observed lack of solubility of PMMA-*b*-C_{60} in solvent mixtures containing less than 60 wt% EA.

3.3. Transmission electron microscopy

Transmission electron microscopy (TEM) was used to confirm the possible morphology of the aggregates. A typical TEM image (magnified) of the PMMA-*b*-C_{60} polymer in 100 wt% EA is shown in Fig. 7(a). The radius of the aggregate is about 75 nm, which is smaller than the particle size in solution (R_h of $\sim$111 nm), which is understandable for dried samples in TEM. Very often, dried aggregates shrunk to yield a smaller size as observed in the TEM. This is particular significant for highly solvated

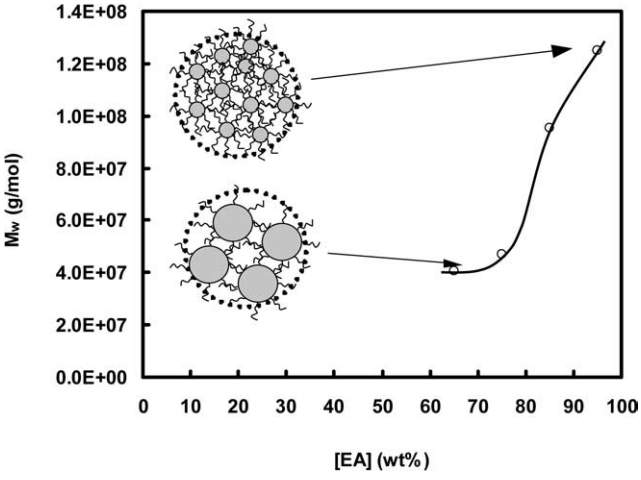

Fig. 6. The possible aggregation mechanism for the formation of PMMA-*b*-C_{60} LCM in different solvent mixtures.

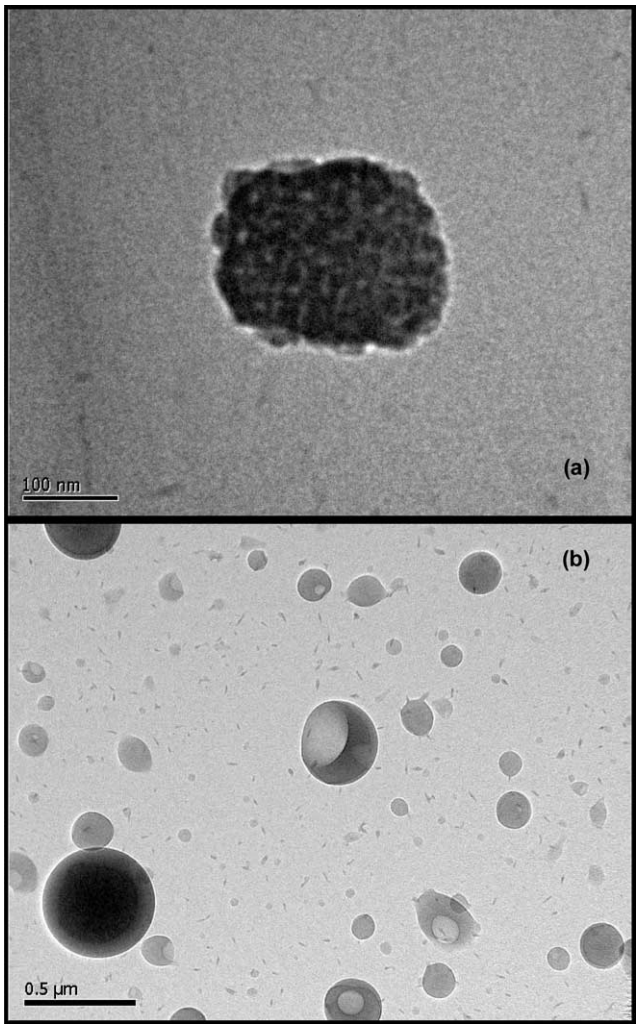

Fig. 7. TEM image of PMMA-*b*-C_{60} aggregates in solvent mixtures: (a) zoom-in TEM image in 100 wt% EA, and (b) in 70 wt% EA.

micellar core as observed in the present study. From the TEM micrograph, we observed many black dot-like structures which correspond to individual micelles within the LCM. The diameter of each 'dot' was estimated to be in the range of 10–20 nm, which corresponds to the spherical PMMA-*b*-C_{60} micelle.

Fig. 7(b) shows the typical TEM image for PMMA-*b*-C_{60} aggregates in 70 wt% EA solution. An interesting morphology similar to bowl-shaped micelles was observed. From the morphology of the microstructure in different solvent compositions observed from the TEM images and the light scattering data for the LCM in different solvent mixtures, the formation of the bowl-shaped structures in the TEM morphology can be elucidated.

In the beginning, the PMMA-*b*-C_{60} polymer self-assembles to form a LCM, with its micellar cores swollen with decalin. Over a period of time, the diffusion of decalin molecules favors the formation of voids resulting in a porous aggregate. The voids coalesce to form a single 'bubble' in the aggregate, and the microstructure

corresponds to a vesicle-like aggregate. We used this terminology since its dimension is much larger than a typical vesicle observed in most self-assembled microstructure. The 'bubble' may also lie off-center due to the random motion of the solvent molecules. As a result, the asymmetric forces acting on it will compel the bubble towards the thinner section of the aggregate. Once the bubble is close to the edge, the surface forces cause the film to thin, which disrupt the membrane. Pieces of the fragments were observed in many of the TEM micrographs. After decalin has diffused from the interior of the LCM to the surrounding bulk solvent, a bowl-shaped micelle is produced induced by surface tension. The structure of the bowl-shaped micelle is transient and in dynamic equilibrium with the other microstructures. Similar bowl-shaped micelles have also been observed by Eisenberg and co-workers in systems of tri-block copolymer of styrene and 5-(*N*,*N*-diethylamino) isoprene [25]. In view of this, PMMA-*b*-C_{60} in mixed solvents and system described by Eisenberg and co-workers shared several similarities, which seem to suggest that there exists a critical condition in which bowl-shaped micelles are produced.

4. Conclusions

The well-defined mono-substituted [60]fullerene containing PMMA was synthesized through ATRP and the chemical composition was confirmed by various analytical techniques. The aggregation behaviors of PMMA-*b*-C_{60} in the EA/decalin solvent mixtures were studied using laser light scattering and transmission electron microscopic techniques. Small amounts of large compound micelles (LCM) are produced via the closed association model, which is found to coexist with the PMMA-*b*-C_{60} unimers and core-shell micelles. With increasing PMMA-*b*-C_{60} concentration in a solvent mixture system, the new equilibrium favors the formation of LCM with a more uniform size distribution and the reduction in proportion of single core-shell micelles and unimers. The dimension of the LCM is independent of decalin content in the solvent mixtures. However, the weight-averaged molecular weights of the LCM decrease with increasing decalin proportion due to the swollen core of each individual core-shell micelle. This produces fewer core-shell micelles in the LCM as compared to another LCM produced in solvent with a lower proportion of decalin. The existence of LCM was also confirmed using the transmission electron microscope. Bowl-shaped micellar structures are produced, which is interpreted based on the proposed mechanism on the microstrutural evolution of LCM in the solvent mixtures.

Acknowledgements

The authors are grateful to Singapore-MIT Alliance and Nanyang Technological University for their financial support to this work.

References

[1] Cravino A, Zerza G, Maggini M, Bucella S, Svensson M, Andersson MR, et al. Chem Commun 2000;24:2487.
[2] Cravino A, Saricifti NS. J Mater Chem 2002;12:1931.
[3] Diederich F, Thilgen C. Science 1996;271:317.
[4] Da RS, Spalluto G, Prato M. Croat Chem Acta 2001;74:743.
[5] Zhu CC, Xu Y, Liu YQ, Zhu DB. J Org Chem 1997;62:1996.
[6] Ford WT, Nishioka T, McCleskey SC, Mourey TH, Kahol P. Macromolecules 2000;33:2413.
[7] Mehrotra S, Nigam A, Malhotra R. Chem Commun 1997;5:463.
[8] Konarev DV, Lyubovskaya RN. Russ Chem Rev 1999;68:19.
[9] Asai M, Fujita N, Shinkai S. Chem Lett 2003;32:186.
[10] Okamura H, Ida N, Minoda M, Komatsu K, Fukuda T. Macromolecules 1998;31:1859.
[11] Bunker CE, Lawson GE, Sun YP. Macromolecules 1995;28:3744.
[12] Dardel B, Guillon D, Heinrich B, Deschenaux R. J Mater Chem 2001; 11:2814.
[13] Okamura H, Terauchi T, Minoda M, Fukuda T, Komatsu K. Macromolecules 1997;30:5279.
[14] Li L, Wang CC, Long ZH, Fu SK. J Polym Sci, Part A: Polym Chem 2000;38:4519.
[15] Lai DT, Neumann MA, Matsumoto M, Sunamoto J. Chem Lett 2000; 1:64.
[16] Riegel IC, Eisenberg A. Langmuir 2002;18:3358.
[17] Song T, Dai S, Tam KC, Lee SY, Goh SH. Polymer 2003;44:2529.
[18] Sano M, Oishi K, Ishi TI, Shinkai S. Langmuir 2000;16:3773.
[19] Okamura H, Ide N, Minoda M, Fukuda T. Macromolecules 1998;31: 1859.
[20] Wang X, Goh SH, Lu ZH, Lee SY, Wu C. Macromolecules 1999;32: 2786.
[21] Yang JW, Li L, Wang CC. Macromolecules 2003;36:6060.
[22] Zhou P, Chen GQ, Hong H, Du FS, Li ZC, Li FM. Macromolecules 2000;33:1948.
[23] Gan LH, Ravi P, Mao BW, Tam KC. J Polym Sci, Part A: Polym Chem 2003;41:2688.
[24] Audouin F, Nuffer R, Mathis CJ. J Polym Sci, Part A: Polym Chem 2004;42:3456.
[25] Riegel IC, Eisenberg A, Petzhold CL, Samios D. Langmuir 2002;18: 3358.